Materials Research. 2019; 22(5): e20190113
DOI: http://dx.doi.org/10.1590/1980-5373-MR-2019-0113

Effects of Heat Treatment and Yb $^{3+}$ Concentration on the Downconversion Emission of Er $^{3+}$ /Yb $^{3+}$ Co-Doped Transparent Silicate Glass-Ceramics

***Ho Kim Dan*[a,b]*, *Tran Duy Tap*[c], *Hieu Nguyen-Truong*[b,d], *Nguyen Minh Ty*[e], *Dacheng Zhou*[f], *Jianbei Qiu*[f]**

[a]*Ceramics and Biomaterials Research Group, Advanced Institute of Materials Science, Ton Duc Thang University, Ho Chi Minh City, Vietnam*
[b]*Faculty of Applied Sciences, Ton Duc Thang University, Ho Chi Minh City, Vietnam*
[c]*Faculty of Materials Science and Technology, University of Science, Viet Nam National University Ho Chi Minh City, 227 Nguyen Van Cu, District 5, Ho Chi Minh, Vietnam*
[d]*Laboratory of Applied Physics, Advanced Institute of Materials Science, Ton Duc Thang University, Ho Chi Minh City, Vietnam*
[e]*Faculty of Natural Sciences, Thu Dau Mot University, Thu Dau Mot 590000, Vietnam*
[f]*Key Laboratory of Advanced Materials of Yunnan Province, School of Materials Science and Engineering, Kunming University of Science and Technology, Kunming 650093, China*

Received: February 07, 2019; Revised: June 28, 2019; Accepted: August 05, 2019

The SiO_2-Al_2O_3-BaF_2-TiO_2-CaF_2 transparent silicate glass-ceramics containing BaF_2 nanocrystals were successfully prepared by heat treatment process through conventional melting method. Effects of heat treatment processes and Yb^{3+} concentration on the downconversion (DC) emission of the co-doped Er^{3+}/Yb^{3+} transparent silicate glass-ceramics were investigated. With the increase of temperatures and times of heat treatment process, the DC emission intensity of the co-doped Er^{3+}/Yb^{3+} glass-ceramics was significantly enhanced. At the same time, with the increase of Yb^{3+} concentration, the value of DC intensity of Er^{3+}/Yb^{3+} co-doped bands centered at 849, 883 and 1533 nm is maximized when the concentration of Yb^{3+} reaches 2.5 mol.%. When the concentration exceed 2.5 mol. %, the DC emission intensity of Er^{3+}/Yb^{3+} co-doped bands centered at 849, 883 and 1533 nm was decreased, owing to the self-quenching effect. It's interesting that the DC emission intensity of Er^{3+}/Yb^{3+} co-doped band centered at 978 nm didn't quench when the Yb^{3+} concentration exceed 2.5 mol. %. At the same time, the DC mechanism and ET processes between Yb^{3+} and Er^{3+} ions were discussed.

Keywords: *Downconversion, BaF_2, heat treatment, glass-ceramics, Er^{3+}/Yb^{3+}.*

1. Introduction

In recent years, the silicon solar cells (Si-SC) are widely used to produce electric energy, it is considered a green and inexhaustible source of energy. Therefore, many studies have developed to enhance the emission spectrum of Si-SC energy [1-4]. Usually, there are two processes that contribute to the increase in emission solar cells (SC) spectrum, which is the downconversion (DC) and the upconversion (UC) of rare earth (RE^{3+}) ions. Among them, the DC emission of the single doped Er^{3+} and the co-doped Er^{3+} with others RE^{3+} ions is a promising way to increase the efficiency spectrum of SC [5-7].

In reality, the solar spectrum is within the wavelength range of 300-2500 nm [8], whereas the band-gap of the Si-SC converts only a small band around (1.000 nm at full efficiency into the electricity. The spectrum below the band-gap is not absorbed at all, and the spectrum above the band-gap is fully absorbed but is converted into electricity with high thermal losses. This spectral mismatch are caused a major loss of energy. Therefore, the researchers have interested in improve DC luminescence intensity of the co-doped RE^{3+} ions to deliver the highest spectrum efficiency for the SC energy [2,9-11].

Among the existing trivalent RE^{3+} ions, the Yb^{3+} has a relatively simple electronic structure of two energy-level manifolds: the $^2F_{7/2}$ ground state and $^2F_{5/2}$ excited state around (1000 nm in the near-infrared (NIR) region, which located just above the band-gap of Si-SC [1,12]. Similar to Yb^{3+}, the Er^{3+} also is one of most efficient ions combining to enhance SC spectrum because it has a favorable energy level structure with $^4I_{15/2} \rightarrow {}^4I_{11/2}$ transition corresponding to NIR emission of about 980 nm. Therefore, enhancement on the DC emission can be achieved by combine of the co-doped Er^{3+}/Yb^{3+}, through energy transfer (ET) process between between Er^{3+} and Yb^{3+} ions. There upon the energy is transferred to two Yb^{3+} ions via a resonant ET process. Finally, the Yb^{3+} ions will emit the two required photons with the band-gap energy of Si-SC [13].

In 2009, L. Aarts et al., [14] have investigated the DC emission for SC in $NaYF_4$: Er^{3+}, Yb^{3+}. This result indicated that the desired DC process from the $^4F_{7/2}$ level has very low efficiency due to fast multi-phonon relaxation from the $^4F_{7/2}$ to $^4S_{3/2}$ level via the intermediate $^2H_{11/2}$ level. Recently, In the paper of M.B. de la Mora et al., [15] mentioned the materials for DC in SC: Perspectives and challenges.

*e -mail: hokimdan@tdtu.edu.vn

Results of this paper affirmed among different options, downconversion is an appealing way to harvest the efficiency in solar cells because it permits to optimize the solar spectrum usage [15]. With the purposed to improved efficiency photoluminescence for the solar cells application. In previous studies, we have investigated enhancement of upconversion emission of Er^{3+}/Yb^{3+} co-doped transparent silicate glass-ceramics containing BaF_2 nanocrystals by effects of Mn^{2+} concentrations [16] and heat treatment processes [17]. In this work, we continues to investigation the effects of the heat treatment processes and Yb^{3+} concentration on the DC emission intensity of the co-doped Er^{3+}/Yb^{3+} transparent silicate glass-ceramics containing BaF_2 nanocrystals. At the same time, the mechanism of DC and ET processes between Yb^{3+} and Er^{3+} ions are also proposed and discussed.

2. Experimental Details

The glasses were prepared according to a conventional melt-quenching method. High-purity SiO_2, Al_2O_3, BaF_2, TiO_2, CaF_2, Er_2O_3, and Yb_2O_3 (99.99%) were used as the starting materials. All glass components (SiO_2, Al_2O_3, BaF_2, TiO_2, CaF_2, Er_2O_3 and Yb_2O_3) were purchased from the Aladdin Industrial Corporation, China. The compositions chosen in the present study are shown in Table 1. Mixtures with a sufficient weight of approximately 10 g, compacted into a platinum crucible, were set in an electric furnace. The electric furnace in this study manufactured by Nabertherm, Germany. After holding at 1500 ºC for 45 min under air atmosphere in an electric furnace, the melts were quenched by putting them onto a polished plate of stainless steel. According to the glass transition temperature (T_g) of differential thermal analysis which was determined by differential scanning calorimeter (DTA-60AH SHIMADZU) with a heating rate of 10 ºC/min under a nitrogen atmosphere.

The samples were cut into the size of 10×10×2 mm^3 and polished for optical measurements. To identify the crystallization phase, XRD (*X-ray diffraction*) analysis was carried out with a powder diffractometer (BRUKER AXS GMBH) using CuKα radiation. The sizes, shape, structure and component compositions of the asprepared nanocrystals were characterized by transmission electron microscopy (TEM, JEM-2100) at 200 kV. The reflectance spectra in the wavelength range of 350-1800 nm were measured on a Hitachi U-4100 spectrophotometer. The DC spectra in the wavelength range of 800-1650 nm and lifetime curves were measured on an Edinburgh Instruments FLS980 fluorescence spectrometer using a μF920 microsecond flash lamp as the excitation source and detected using a liquid-nitrogen-cooled PbS detector upon excitation at 410 nm. All spectral, DTA, XRD, TEM measurements were conducted at ambient temperatures.

3. Results and Discussion

To characterize the thermal stability of the prepared SiO_2-Al_2O_3-BaF_2-TiO_2-CaF_2 glass system, a DTA curve of SEY-1 glass sample was measured and showed in Fig.1.

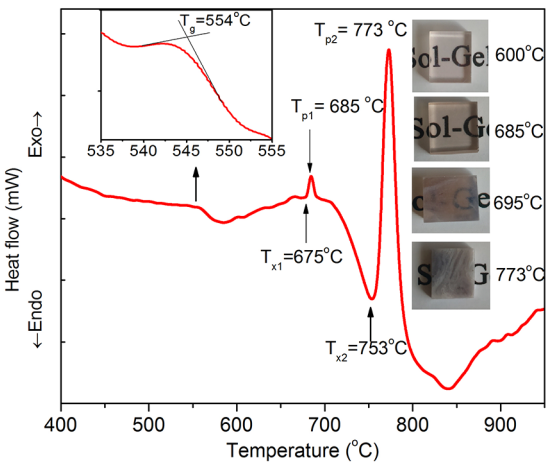

Figure 1. The DTA curves of SEY-0.2E2.5Y glasses.

Table 1. Chemical composition of SiO_2–Al_2O_3–BaF_2–TiO_2–CaF_2–Er_2O_3–Yb_2O_3 glasses (in mol. %)

Glasses name		Composition ratios of reagents (in mol. %)						
		SiO_2	Al_2O_3	BaF_2	TiO_2	CaF_2	Er_2O_3	Yb_2O_3
SEY-1	SEY-0.2E0Y	45	19.8	20	10	5	0.2	0
	SEY-0.2E1Y	45	18.8	20	10	5	0.2	1
	SEY-0.2E1.5Y	45	18.3	20	10	5	0.2	1.5
	SEY-0.2E2Y	45	17.8	20	10	5	0.2	2
	SEY-0.2E2.5Y	45	17.3	20	10	5	0.2	2.5
	SEY-0.2E3Y	45	16.8	20	10	5	0.2	3
SEY-2	SEY-0.1E2.5Y	45	17.4	20	10	5	0.1	2.5
	SEY-0.3E2.5Y	45	17.2	20	10	5	0.3	2.5
	SEY-0.5E2.5Y	45	17	20	10	5	0.5	2.5
	SEY-0.8E2.5Y	45	16.7	20	10	5	0.8	2.5
	SEY-1E2.5Y	45	16.5	20	10	5	1	2.5

As can be seen in this figure, three temperature parameters: the glass transition temperature (T_g) was located around 554 ºC, the crystallization onset temperature (T_{x1} = 675 ºC), two crystallization peaks temperatures ($T_{p1,}$ T_{p2}) are located around 685 ºC and 773 ºC, respectively. Therefore, the transparent silicate glass-ceramics can be prepared by heat-treat in the first crystallization peak near 665 ºC, by controlling the appropriate crystallization temperature and process. Besides, between ~710ºC and 773 ºC, an endothermic reaction occurs. It's also the crystallization onset temperature (T_{x2}) and the T_{x2} is determined value around 753ºC. The difference ΔT between the crystallization onset temperature T_{x1} and the glass transition temperature T_g ($\Delta T = T_{x1} - T_g$) is used as a rough indicator of glass thermal stability, and the ΔT = 675 ºC - 554 ºC = 121ºC > 100 ºC indicating the prepared glass is stable and suitable for applications such as fiber amplifiers and solar cells, etc. Based on the analysis results of the DTA curve, all the prepared glasses were heat-treated within the range of 665ºC to 773 ºC. However, when glass-ceramics samples heat-treated up to 695 ºC, the glass-ceramics sample is no longer transparent glass-ceramics. The optical images of glass-ceramics samples heat treatment at ~600, 685, 695 and 773 ºC as shown in inset of Fig. 1. Therefore, in this study, we had chosen heat treatment temperatures for transparent silicate glass-ceramics samples within the range of 600-685 ºC. Polished SEY-0.2E2.5Y glass sample was then heat treated at four different temperatures: 600, 630, 660 and 685 ºC, which were selected to carry out heat treatment for 5 h to form transparent silicate glass-ceramics and the fabricated samples were named as SEY-0.2E2.5Y-600, SEY-0.2E2.5Y-630, SEY-0.2E2.5Y-660, and SEY-0.2E2.5Y-685, respectively. At the same time, the polished SEY-0.2E2.5Y glass samples were selected to carry out heat treatment at 685 ºC for different times 10, 15, 20, 25 and 30 h to form transparent silicate glass-ceramics and the fabricated samples were named as SEY-0.2E2.5Y-10h, SEY-0.2E2.5Y-15h, SEY-0.2E2.5Y-20h, SEY-0.2E2.5Y-25h, and SEY-0.2E2.5Y-30h, respectively.

The transparent silicate glass-ceramics was prepared and the nanocrystals structures in the glass-ceramics were monitored by XRD. The XRD patterns of glass-ceramics after heat treatment at different temperatures are shown in Fig. 2 (a). From the results of Fig. 2(a) shows when the increase of processing temperature from 600 up to 685 ºC, crystal size of BaF_2 nanocrystals was increased from 10.7 up to 17.9 nm. Relationship between crystal size with the heat treatment temperatures are shown in the Fig. 2(b).

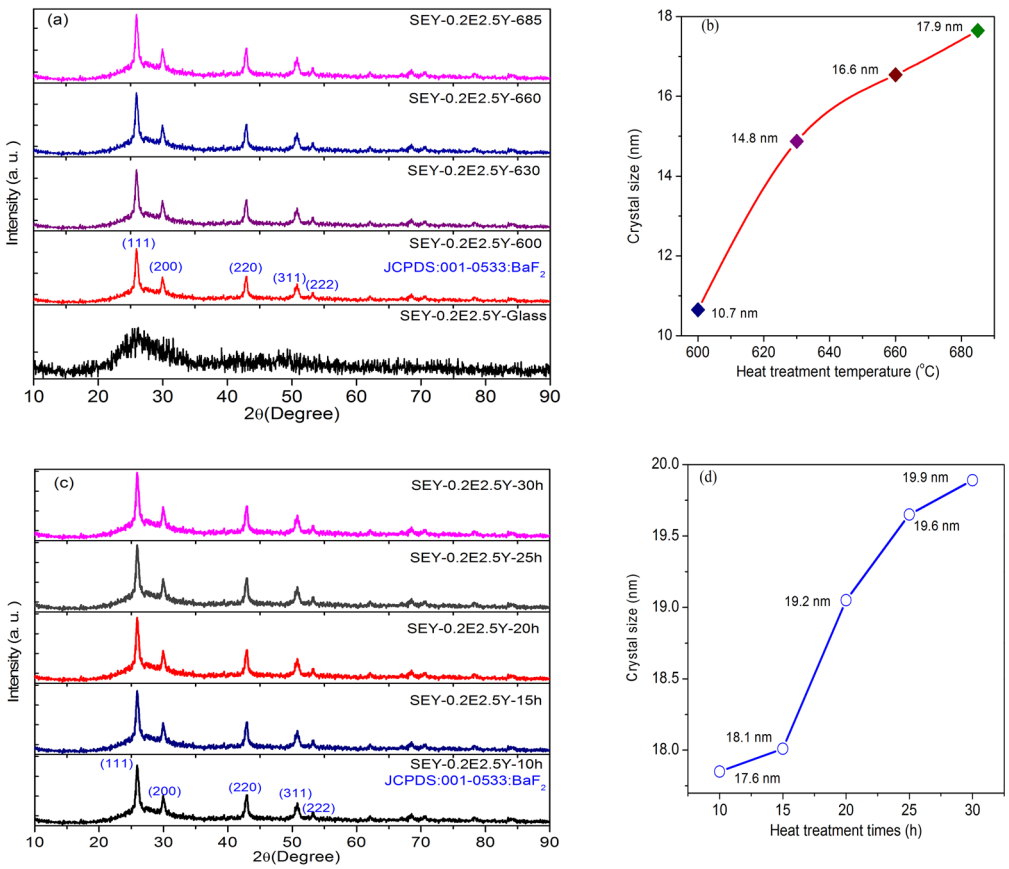

Figure 2. (a) XRD patterns of SEY-0.2E2.5Y glass sample and SEY-0.2E2.5Y-600, SEY-0.2E2.5Y-630, SEY-0.2E2.5Y-660 and SEY-0.2E2.5Y-685 transparent glass-ceramics samples; (b) Relationship between crystal size with the heat treatment temperatures; (c) XRD patterns of the SEY-0.2E2.5Y-10h, SEY-0.2E2.5Y-15h, SEY-0.2E2.5Y-20h, SEY-0.2E2.5Y-25h and SEY-0.2E2.5Y-30h transparent glass-ceramics samples; (d) Relationship between crystal size with the heat treatment times.

Fig. 2 (a) XRD patterns of SEY-0.2E2.5Y glass sample and SEY-0.2E2.5Y-600, SEY-0.2E2.5Y-630, SEY-0.2E2.5Y-660 and SEY-0.2E2.5Y-685 transparent glass-ceramics samples; (b) Relationship between crystal size with the heat treatment temperatures; (c) XRD patterns of the SEY-0.2E2.5Y-10h, SEY-0.2E2.5Y-15h, SEY-0.2E2.5Y-20h, SEY-0.2E2.5Y-25h and SEY-0.2E2.5Y-30h transparent glass-ceramics samples; (d) Relationship between crystal size with the heat treatment times.

Also from the result of the Fig. 2(a), the precursor glass sample presents a broad diffraction curve characteristic of the amorphous state, while in the patterns of transparent silicate glass-ceramics, the intense diffraction peaks are clearly observed, indicating that microcrystallites are successfully precipitated during thermal treatment. The diffraction pattern of the crystalline element is typical of a face-centered-cubic and these diffraction peaks around 2θ(degree) = 26º, 30º, 43º, 50º and 53º can be assigned respectively to the (111), (200), (220), (311) and (222) planes of the BaF_2 cubic phase.

The XRD patterns of glass-ceramics after heat treatment at different times are shown in Fig. 2 (c). From the results of Fig. 2(c) shows when the increase of processing times from 10 up to 30h, crystal size of BaF_2 nanocrystals was increased from 17.6 up to 19.9 nm. Relationship between crystal size with the heat treatment times are shown in the Fig. 2(d).

The crystallites size D for a given (hkl) plane was estimated from the XRD patterns following the Scherrer equation:

$$D = \frac{\lambda \times K}{\beta \times \cos\theta} \quad (1)$$

Where K = 0.9, λ is the wavelength of the incident XRD [CuK_α (λ = 0.154056 nm)], β is the FWHM in radians and θ is the diffraction angle for the (hkl) plane. By using Debye-Scherrer equation, the average of BaF_2 crystallites size of SEY-0.2E2.5Y-600, SEY-0.2E2.5Y-630, SEY-0.2E2.5Y-660, SEY-0.2E2.5Y-685, SEY-0.2E2.5Y-10h, SEY-0.2E2.5Y-15h, SEY-0.2E2.5Y-20h, SEY-0.2E2.5Y-25h and SEY-0.2E2.5Y-30h transparent glass-ceramics samples has been calculated and displayed in the Figs. 2 (c&d). The results calculation of BaF_2 crystallites size and the relationship between the crystal size with the heat-treated different temperatures and times in the glass-ceramics are shown in Figs. 2 (c & d). Clearly, in this figure, the increase of the heat treatment temperatures and times were led to the crystal size increased, similar to the result of our previous works [17-19].

The TEM image of SEY-0.2E2.5Y-685 transparent silicate glass-ceramics sample is shown in Fig. 3. From result of Fig. 3, it demonstrates that the BaF_2 nanocrystals were distributed homogeneously among the glass matrix and the mean sizes of nanocrystals were about 18-19 nm, which was similar to those calculated by Debye-Scherrer equation. The HRTEM image of the SEY-0.2E2.5Y-685 transparent silicate glass-ceramics sample is shown in inset of Fig. 3. As from this figure, the lattice spacing of (111) was estimated about 0.334 nm.

The reflectance spectra of the Er^{3+}/Yb^{3+} co-doped SEY-0.2E2.5Y glass and SEY-0.2E2.5Y-600, SEY-0.2E2.5Y-630, SEY-0.2E2.5Y-660 and SEY-0.2E2.5Y-685 transparent glass-ceramics samples within the range of 350 to 1800 nm are exhibited in Fig. 4. The reflectance bands corresponding to transitions from the ground-state ($^4I_{15/2}$) to excited states: $^4G_{11/2}$, $^2H_{11/2}$, ($^4F_{3/2}$, $^4F_{5/2}$), $^4F_{7/2}$, $^2H_{11/2}$, $^4S_{3/2}$, $^4F_{9/2}$, $^4I_{9/2}$, $^4I_{11/2}$ and $^4I_{13/2}$ transitions of the Er^{3+} and $^2F_{7/2} \rightarrow {}^2F_{5/2}$ of the Yb^{3+} ions, respectively, were observed. Furthermore, the reflectance intensity at $^4F_{5/2}$, $^4F_{7/2}$, $^2H_{11/2}$, $^4S_{3/2}$, $^4F_{9/2}$, $^4I_{9/2}$, $^4I_{11/2}$, $^4I_{13/2}$ states of the Er^{3+} and $^2F_{5/2}$ of the Yb^{3+} ions were increased with the increase of heat treatment temperatures from 600 to 685 ºC.

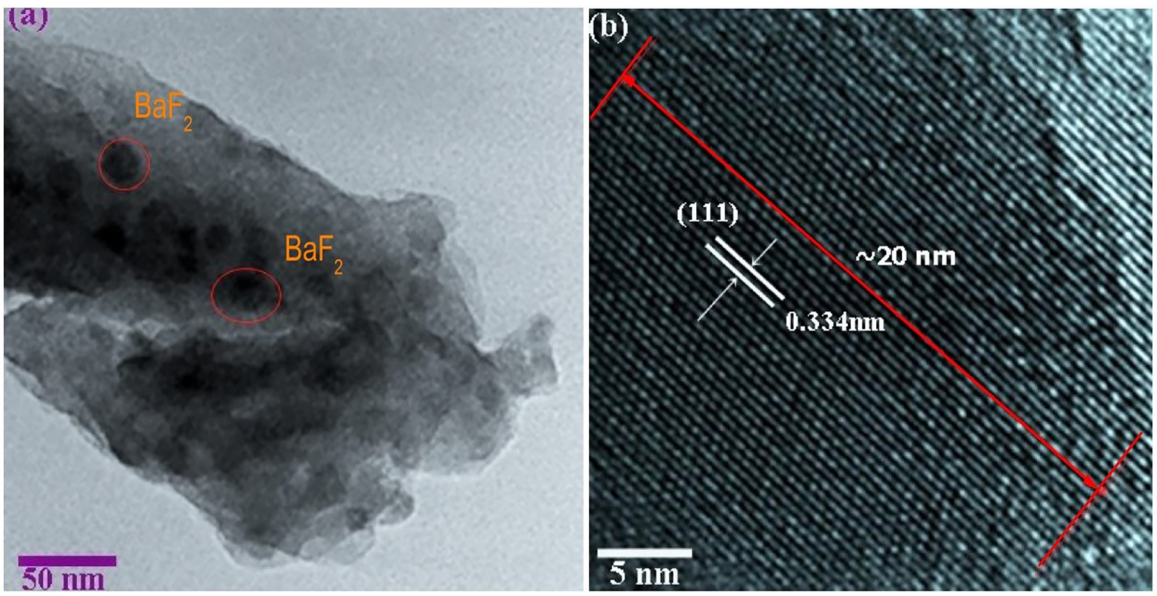

Figure 3. (a) TEM image of SEY-0.2E2.5Y-685 transparent silicate glass-ceramics sample; (b) HRTEM image of SEY-0.2E2.5Y-685 transparent silicate glass-ceramics sample.

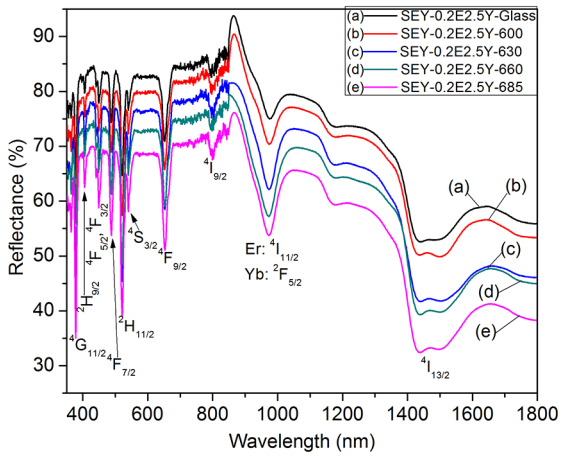

Figure 4. Reflectance spectra of Er^{3+}/Yb^{3+} co-doped in SEY-0.2E2.5Y-glass, SEY-0.2E2.5Y-600, SEY-0.2E2.5Y-630, SEY-0.2E2.5Y-660, and SEY-0.2E2.5Y-685 transparent glass-ceramics samples.

Figure 5 shows DC emission spectra of the SEY-0.2E2.5Y-glass, SEY-0.2E2.5Y-600, SEY-0.2E2.5Y-630, SEY-0.2E2.5Y-660 and SEY-0.2E2.5Y-685 transparent glass-ceramics samples under excitation 410 nm in resonance with the $^2H_{9/2}$ (Er^{3+}) level. In contrast to the slight DC luminescence observed through the precursor glass, the strong DC emission intensity of the Er^{3+}/Yb^{3+} co-doped bands centered at 824 nm ($^2H_{9/2} \rightarrow {}^4I_{11/2}$), 849 nm ($^2H_{11/2} \rightarrow {}^4I_{13/2}$), 883 nm ($^4S_{3/2} \rightarrow {}^4I_{13/2}$), 918 nm ($^4F_{7/2} \rightarrow {}^4I_{11/2}$), 978 nm ($^4I_{11/2} \rightarrow {}^4I_{15/2}$ of the Er^{3+} and $^2F_{5/2} \rightarrow {}^2F_{7/2}$ of the Yb^{3+}), 1265 nm ($^4S_{3/2} \rightarrow {}^4I_{11/2}$), 1533 nm ($^4I_{13/2} \rightarrow {}^4I_{15/2}$) were observed in the glass-ceramics after heat treatment process changing temperatures [18]. The reasons contributing to the increase of the DC emission intensity: in the case of the specimens after heat treatment, the Er^{3+} and Yb^{3+} ions practically dispersive into precipitated nanocrystal, the Er^{3+} and Yb^{3+} ions are condensed in the glass-ceramics, so that the distances between the Er^{3+} and Yb^{3+} become closer and consequently result in increasing of the DC emission intensity [20].

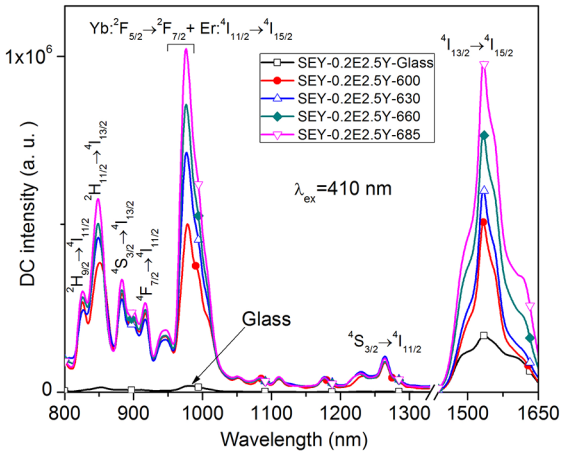

Figure 5. DC emission spectra of SEY-0.2E2.5Y-glass, SEY-0.2E2.5Y-600, SEY-0.2E2.5Y-630, SEY-0.2E2.5Y-660 and SEY-0.2E2.5Y-685 transparent glass-ceramics samples.

The DC emission spectra of the SEY-0.2E2.5Y-10h, SEY-0.2E2.5Y-15h, SEY-0.2E2.5Y-20h, SEY-0.2E2.5Y-25h, and SEY-0.2E2.5Y-30h transparent glass-ceramics samples, under excitation 410 nm are shown in Fig. 6. Similar in the case of changing heat treatment temperatures, the DC emission intensity of the Er^{3+}/Yb^{3+} co-doped bands centered at 824, 849, 883, 918, 978, 1265 and 1533 nm were strongly increased with the increase of heat treatment times from 10 to 30 h. These results confirms that the heat treatment processes greatly affects the DC emission intensity of Er^{3+}/Yb^{3+} co-doped transparent silicate glass-ceramics.

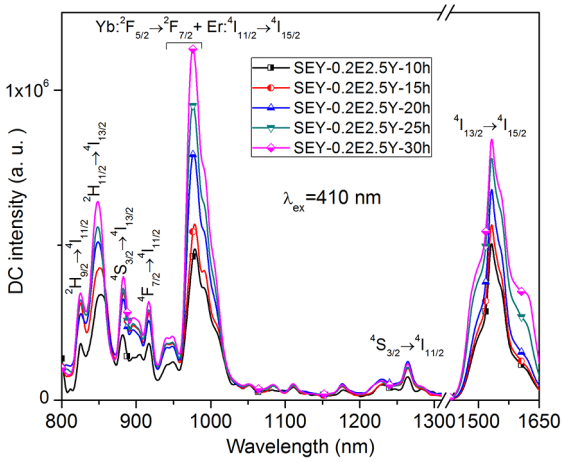

Figure 6. DC emission spectra of SEY-0.2E2.5Y-10h, SEY-0.2E2.5Y-15h, SEY-0.2E2.5Y-20h, SEY-0.2E2.5Y-25h, and SEY-0.2E2.5Y-30h transparent glass-ceramics samples.

Furthermore, the effect of Yb^{3+} concentration on the DC emission intensity of Er^{3+}/Yb^{3+} co-doped transparent silicate glass-ceramics were also presented follows. The DC emission spectra of SEY-0.2E0Y, SEY-0.2E1.0Y, SEY-0.2E1.5Y, SEY-0.2E2.0Y, SEY-0.2E2.5Y and SEY-0.2E3.0Y transparent glass-ceramics samples, under 410 nm excitation are shown in Fig. 7. As shown in the Fig. 7, in the DC process, the Yb^{3+} ions act as an efficient sensitizer. While Er^{3+} fixed concentration, with the increase of Yb^{3+} concentration, the DC emission intensity of Er^{3+}/Yb^{3+} co-doped bands centered at 849, 883 and 1533 nm were strongly increased and reaches its maximum value when the content of Yb_2O_3 is 2.5 mol. %. When the concentration exceed 2.5 mol. %, the DC emission intensity of Er^{3+}/Yb^{3+} co-doped bands centered at 849, 883 and 1533 nm was decreased. This result may be owing to the reasons mainly of the self-quenching effect can be attributed to the cluster or the ions pair between the Yb^{3+} ions is possibly formed in high the Yb^{3+} concentration [21]. Further, the increase of Yb^{3+} concentration has enhanced the probability of interaction between the Yb^{3+} ions and some impurity, such as OH^- impurities was born from atmospheric moisture during melting [22]. Therefore, the Yb^{3+} could not effectively absorb the pumping energy leading to the quenching of the DC emission intensities.

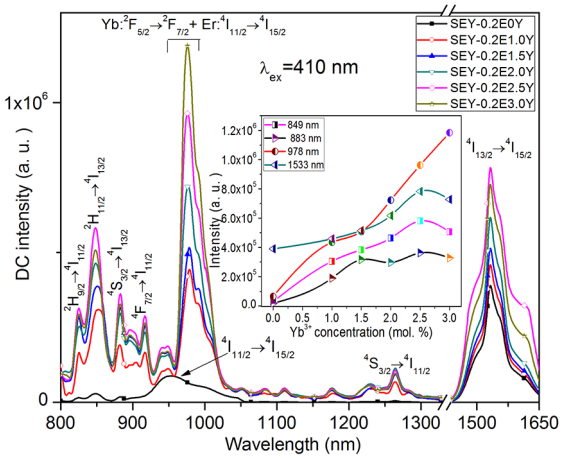

Figure 7. DC emission spectra of SEY-0.2E0Y, SEY-0.2E1.0Y, SEY-0.2E1.5Y, SEY-0.2E2.0Y, SEY-0.2E2.5Y and SEY-0.2E3.0Y transparent glass-ceramics samples.

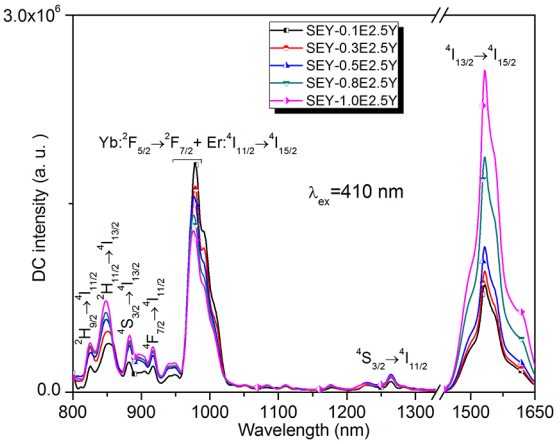

Figure 8. DC emission spectra of SEY-0.1E2.5Y, SEY-0.3E2.5Y, SEY-0.5E2.5Y, SEY-0.8E2.5Y and SEY-1.0E2.5Y transparent glass-ceramics samples.

It is interesting that the DC emission intensity band centered 978 nm, corresponding to the transitions: $^4I_{11/2} \rightarrow {}^4I_{15/2}$ of Er^{3+} and $^2F_{5/2} \rightarrow {}^2F_{7/2}$ of Yb^{3+} didn't quench when the Yb^{3+} concentration excess 2.5 mol. % (see inset of Fig. 7). The strong DC emission intensity band around 978 nm consists in two contributions: (i) the $^4I_{11/2} \rightarrow {}^4I_{15/2}$ transition of Er^{3+} ions and (ii) the $^2F_{5/2} \rightarrow {}^2F_{7/2}$ transition of Yb^{3+} ions. On the other hand, the increase of the DC emission intensity bands at 849, 883 and 1533 nm can be explained by the following reasons: Firstly, we deem that the ET from $^2F_{5/2} \rightarrow {}^2F_{7/2}$ transition of Yb^{3+} to $^4I_{11/2} \rightarrow {}^4I_{15/2}$ and $^4F_{9/2} \rightarrow {}^4I_{13/2}$ transitions of the Er^{3+} might be occurred. Secondly, the cross-relaxation (CR) may be occur between two neighboring Er^{3+} ions [$^4F_{9/2}$-$^4I_{13/2}$]; [$^2H_{9/2}$-$^4F_{9/2}$], the efficiency of the ET strongly depends on the distance of two Er^{3+} ions. The mechanism of the ET from Yb^{3+} to Er^{3+} ions and CR from Er^{3+} to Er^{3+} ions was suggested as follows:

$$^2F_{5/2}(Yb^{3+}) + {}^4I_{11/2}(Er^{3+}) \rightarrow {}^2F_{7/2}(Yb^{3+}) + {}^4I_{15/2}(Er^{3+}) \text{ (ET1)}$$

$$^2F_{5/2}(Yb^{3+}) + {}^4I_{13/2}(Er^{3+}) \rightarrow {}^2F_{7/2}(Yb^{3+}) + {}^4F_{9/2}(Er^{3+}). \text{ (ET2)}$$

$$^4F_{9/2}(Er^{3+}) + {}^2H_{9/2}(Er^{3+}) \rightarrow {}^4I_{13/2}(Er^{3+}) + {}^4F_{9/2}(Er^{3+}). \text{ (CR).}$$

In addition, a variation of the molar concentration of Er^{3+} ions while keeping the concentration of Yb^{3+} ions in transparent silicate glass-ceramics composition was also given for comparison in the second component of SEY-2 transparent glass-ceramics sample. The DC emission of SEY-0.1E2.5Y, SEY-0.3E2.5Y, SEY-0.5E2.5Y, SEY-0.8E2.5Y, and SEY-1.0E2.5Y glass-ceramics samples under excitation 410 nm are shown in Fig. 8. From results in Figure 8, the DC emission intensity bands centered at 824 nm ($^2H_{9/2} \rightarrow {}^4I_{11/2}$), 849 nm ($^2H_{11/2} \rightarrow {}^4I_{13/2}$), 883 nm ($^4S_{3/2} \rightarrow {}^4I_{13/2}$), 918 nm ($^4F_{7/2} \rightarrow {}^4I_{11/2}$), 1265 nm ($^4S_{3/2} \rightarrow {}^4I_{11/2}$) and 1533 nm ($^4I_{13/2} \rightarrow {}^4I_{15/2}$) originated from Er^{3+} ions were significantly increased with the increase of Er^{3+} ions. In contrast, the DC emission intensity band centered around 978 nm, corresponding to the transitions: $^4I_{11/2} \rightarrow {}^4I_{15/2}$ transition of Er^{3+} and $^2F_{5/2} \rightarrow {}^2F_{7/2}$ transition of Yb^{3+} decreased with increasing molar concentration of Er^{3+} ions. This phenomenon can be explained by these reasons: Firstly, as the molarity of Er^{3+} ions increased, the increased luminescent centers lead the emission intensity bands centered at 824, 849, 883, 918, 1265 and 1533 nm significantly increased. Secondly, the possible ET from Yb^{3+} to Er^{3+} ions, contribute to the emission intensity bands centered at 824, 849, 883, 918, 1265 and 1533 nm improved while emission intensity bands centered at 978 nm decreased. The mechanism of the ET from Yb^{3+} to Er^{3+} ions was proposed as above section.

The DC emission mechanism of Er^{3+}/Yb^{3+} co-doped glass-ceramics are depicted schematically in Fig. 9.

Fig. 9 Mechanism for DC processes of the Er^{3+}/Yb^{3+} co-doped in SEY-1 glass-ceramics, under excitation 410 nm.

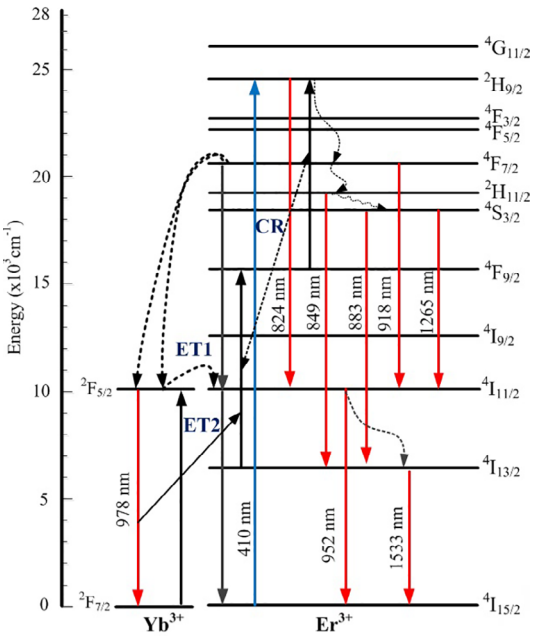

Figure 9. Mechanism for DC processes of the Er^{3+}/Yb^{3+} co-doped in SEY-1 glass-ceramics, under excitation 410 nm.

First of all, the Er^{3+} ions were the excited to the $^2H_{9/2}$ level under excitation at 410 nm. From the $^2H_{9/2}$ level, the Er^{3+} ions decay radiative to the $^4I_{11/2}$ state generating the DC emission around at 824 nm, and then quickly relaxes to the $^4F_{7/2}$ level with multi-phonon relaxing process [23]. The next step, from the $^4F_{7/2}$ level, the Er^{3+} ions decay radiative to the $^4I_{11/2}$ state generating the DC emission around 918 nm, and the $^4F_{7/2}$ level relaxes to the $^2H_{11/2}$ and further relaxation to the $^4S_{3/2}$ levels. At the same time, the cooperative energy transfer (CET) process from one Er^{3+} ion to two neighboring Yb^{3+} ions occurs via cooperative dipole-dipole interaction. Subsequently, the ET from $^2F_{5/2} \rightarrow {}^2F_{7/2}$ transition of Yb^{3+} to $^4I_{11/2} \rightarrow {}^4I_{15/2}$ and $^4F_{9/2} \rightarrow {}^4I_{13/2}$ transitions of Er^{3+} were occurred. And after the ET process, the Yb^{3+} emission is observed around 978 nm corresponding to the $^2F_{5/2} \rightarrow {}^2F_{7/2}$ transition. From the $^2H_{11/2}$ level, the Er^{3+} ions decay radiative to the $^4I_{11/2}$ state generating the DC emission band at 849 nm. Similarly, from the $^4S_{3/2}$ level, the Er^{3+} ions decay radiative to $^4I_{13/2}$ and $^4I_{11/2}$ states generating the DC emissions bands around 883 and 1265 nm, respectively [24]. The major contribution to the DC emission at 1533 nm is attributed to the $^4I_{13/2} \rightarrow {}^4I_{15/2}$ transition as shown in Fig. 9.

Furthermore, the fluorescence lifetimes of Yb^{3+} have been measured in SEY-0.1E2.5Y, SEY-0.3E2.5Y, SEY-0.5E2.5Y, SEY-0.8E2.5Y, and SEY-1.0E2.5Y transparent glass-ceramics samples to have a further evidence of energy transfer from Yb^{3+} to Er^{3+}. The fluorescence lifetimes τ of Yb^{3+} at $^2F_{5/2} \rightarrow {}^2F_{7/2}$ under 410 nm excitation were measured and were presented in Fig. 10. The fluorescence lifetime was monitored at 1000 nm to avoid the luminescence owing to the $^4I_{11/2} \rightarrow {}^4I_{15/2}$ (Er^{3+}) emission. Decay curves were well calculated as a double-exponential luminescence decay by using equation [25]:

$$I(t) = A_1 . \exp\left(\frac{-t}{t_1}\right) + A_2 . \exp\left(\frac{-t}{t_2}\right) \qquad (2)$$

Where I(t) is the luminescence intensity; A_1 and A_2 are fitting constants; t is the time; τ_1 and τ_2 are short and long decay lifetimes for exponential components, respectively. By using these parameters, average photoluminescence lifetimes (τ^*) for SEY-0.1E2.5Y, SEY-0.3E2.5Y, SEY-0.5E2.5Y, SEY-0.8E2.5Y and SEY-1.0E2.5Y transparent glass-ceramics samples can be resolved and calculated by using equation [26]:

$$t^* = \frac{A_1 t_1^2 + A_2 t_2^2}{A_1 t_1 + A_2 t_2} \qquad (3)$$

Average decay lifetimes of SEY-0.1E2.5Y, SEY-0.3E2.5Y, SEY-0.5E2.5Y, SEY-0.8E2.5Y, and SEY-1.0E2.5Y transparent glass-ceramics samples has been calculated to be about 32.5, 30.9, 29.8, 27.6 and 25.4 μs, respectively. Decay lifetimes for Yb^{3+} at ($^2F_{5/2} \rightarrow {}^2F_{7/2}$) transition were found to decrease with increase of Er^{3+} concentration, this result confirms that the strong evidence for the ET from Yb^{3+} to Er^{3+} ions [14,27].

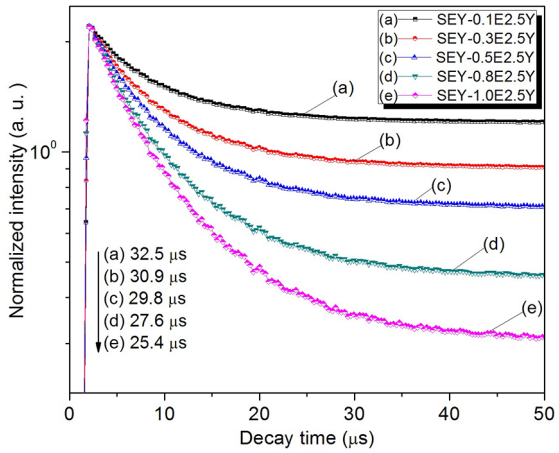

Figure 10. Decay lifetimes τ of Yb^{3+} at $^2F_{5/2} \rightarrow {}^2F_{7/2}$ under excitation 410 nm

4. Conclusions

In study of this article, the effects of heat treatment and Yb^{3+} concentration on the DC emission of Er^{3+}/Yb^{3+} co-doped in transparent silicate glass-ceramics containing BaF_2 nanocrystals were successfully investigated. Comparison with the precursor glass, the DC luminescence of Er^{3+}/Yb^{3+} co-doped transparent glass-ceramics has significantly enhanced after heat treatment process changing temperatures and times. With the increase of Yb^{3+} concentration, the DC emission intensity of Er^{3+}/Yb^{3+} co-doped bands centered at 849, 883 and 1533 nm were strongly increased and reaches its maximum at 2.5 mol. % Yb^{3+} concentration.

When the concentration exceed 2.5 mol. %, the DC emission intensity of Er^{3+}/Yb^{3+} co-doped bands centered at 849, 883 and 1533 nm was decreased, owing to the self-quenching effect. Whereas the DC emission intensity band centered 978 nm, corresponding to the transitions: $^4I_{11/2} \rightarrow {}^4I_{15/2}$ of Er^{3+} and $^2F_{5/2} \rightarrow {}^2F_{7/2}$ of Yb^{3+} didn't quench when the Yb^{3+} concentration exceed 2.5 mol. %. At the same time, we deem that there was possibly an energy transition process from the $^2F_{5/2} \rightarrow {}^2F_{7/2}$ transition of Yb^{3+} to the $^4I_{11/2} \rightarrow {}^4I_{15/2}$ and $^4F_{9/2} \rightarrow {}^4I_{13/2}$ transitions of Er^{3+} ions. In addition, the data presented for this study might provide useful information for further development of the DC in transparent silicate glass-ceramics associated with the ET between Yb^{3+} and Er^{3+} ions. These materials are promising for applications in enhancing conversion efficiency of SC.

5. Acknowledgments

This research is funded by Vietnam National Foundation for Science and Technology Development (NAFOSTED) under grant number 103.03-2019.56

6. References

1. Wei XT, Huang S, Chen YH, Guo CX, Yin M, Xu W. Energy transfer mechanisms in Yb^{3+} doped YVO_4 near-infrared downconversion phosphor. *Journal of Applied Physics*. 2010;107(10):103107.

2. Spitzer MB, Jenssen HP, Cassanho A. An approach to downconversion solar cells. *Solar Energy Materials and Solar Cells*. 2013;108:241-245 .

3. Elleuch R, Salhi R, Al-Quraishi SI, Deschanvres JL, Maâlej R. Efficient antireflective downconversion Er^{3+}-doped ZnO/Si thin film. *Phys. Lett*. A. 2014;378:1733-1738.

4. Cao XQ, Wei T, Chen YH, Yin M, Guo CX, Zhang WP. Increased downconversion efficiency and improved near infrared emission by different charge compensations in $CaMoO_4$:Yb^{3+} powders. *Journal of Rare Earth*. 2011;29(11):1029-35.

5. Van der Ende BM, Aarts L, Meijerink A. Near-infrared quantum cutting for photovoltaics. *Adv Mater*. 2009;21(30):3037-3128.

6. Lakshminarayana G, Qiu J. Near-infrared quantum cutting in RE^{3+}/Yb^{3+} (RE = Pr, Tb, and Tm): GeO_2-B_2O_3-ZnO-LaF_3 glasses via downconversion. *Journal of Alloys and Compounds*. 2009;481(1-2):582-589.

7. Trupke T, Green MA. Improving solar cell efficiencies by down-conversion of high-energy photons. *Journal of Applied Physics*. 2002;92:1668-1674.

8. Thuillier G, Hersé M, Labs D, Foujols T, Peetermans W, Gillotay D, Simon PC, Mandel H. The solar spectral irradiance from 200 to 2400 nm as measured by the solspec spectrometer from the atlas and eureca missions. *Solar Physics*. 2003;214(1):1-22.

9. Zhao L, Han L, Wang Y. Efficient near-infrared downconversion in $KCaGd(PO_4)_2$:Ce^{3+},Yb^{3+}. *Optical Materials Express*. 2014;4(7):1456-64.

10. Bera D, Qian L, Tseng TK, Holloway PH. Quantum dots and their multimodal applications: A Review. *Materials (Basel)*. 2010;3(4):2260-2345.

11. Richards BS. Luminescent layers for enhanced silicon solar cell performance, Down-conversion. *Solar Energy Materials and Solar Cells*. 2006;90(9):1189-207.

12. Teng Y, Zhou J, Liu X, Ye S, Qiu J. Efficient broadband near-infrared quantum cutting for solar cells. *Optics Express*. 2010;18(9):9671-6.

13. Aarts L, Jaeqx S, Van der En BM, Meijerink A. Downconversion for the Er^{3+}, Yb^{3+} couple in KPb_2Cl_5-A low-phonon frequency host. *Journal of Luminescence*. 2011;131:608-613.

14. Aarts L, Van der Ende BM, Meijerink A. Downconversion for solar cells in $NaYF_4$: Er, Yb. *Journal of Applied Physics*. 2009;106(2):023522.

15. Moraa MB, Amelines-Sarriab O, Monroyd BM, Hernández-Pérez CD, Lugo JE. Materials for downconversion in solar cells: Perspectives and challenges. *Solar Energy Materials & Solar Cells*. 2017;165:59-71.

16. Dan HK, Zhou D, Wang R, Jiao Q, Yang Z, Song Z, Yu X, Qiu J. Effect of Mn^{2+} ions on the enhancement red upconversion emission of $Mn^{2+}/Er^{3+}/Yb^{3+}$ tri-doped in transparent glass-ceramics. *Optics & Laser Technology*. 2014;64:264-268.

17. Dan HK, Zhou D, Wang R, Hau TM, Jiao Q, Yu X, Qiu J. Upconversion of Er^{3+}/Yb^{3+} co-doped transparent glass-ceramics containing Ba_2LaF_7 nanocrystals. *Journal of Rare Earth*. 2013;31(9):843-848.

18. Santana-Alonso A, Yanes AC, Méndez-Ramos J, Del-Castillo J, Rodríguez VD. Sol-gel transparent nano glass-ceramics containing Eu^{3+}-doped $NaYF_4$ nanocrystals. *Journal of Non-Crystalline Solids*. 2010;356(18-19):933-936.

19. Dan HK, Zhou D, Wang R, Yu X, Jiao Q, Yang Z, Song Z, Qiu J. Energy transfer and UC emission of $Er^{3+}/Tb^{3+}/Yb^{3+}$ co-doped transparent glass-ceramics containing Ba_2LaF_7 nanocrystals under heat treatment. *Optical Materials*. 2014;36(3):639-644.

20. Kawamoto Y, Kanno R, Qiu J. Upconversion luminescence of Er^{3+} in transparent SiO_2-PbF_2-ErF_3 glass-ceramics. *Journal of Materials Science*. 1998;33(1):63-67.

21. Shi DM, Zhang QY, Yang GF, Zhao C, Yang Z, Jiang ZH. Frequency upconversion luminescence in Tm^{3+}/Yb^{3+}- and Ho^{3+}/Yb^{3+}-codoped Ga_2O_3-GeO_2-Bi_2O_3-PbO glasses. *Journal of Alloys and Compounds*. 2008;466(s1-2):373-376.

22. Meneses-Nava MA, Barbosa-García O, Maldonado JL, Ramos-Ortíz G, Pichardo JL, Torres-Cisneros M, García-Hernández M, García-Murillo A, Carrillo-Romo FJ. Yb^{3+} quenching effects in co-doped polycrystalline $BaTiO_3$:Er^{3+}, Yb^{3+}. *Optical Materials*. 2008;31(2):252-260.

23. Tikhomirov VK, Rodri´guez VD, Me´ndez-Ramos J, Del-Castillo J, Kirilenko D, Van Tendeloo D, Moshchalkov VV. Optimizing Er/Yb ratio and content in Er-Yb co-doped glass-ceramics for enhancement of up- and down-conversion luminescence. *Solar Energy Materials and Solar Cells*. 2012;100:209-215.

24. Shi Y, Zhu G, Mikami M, Shimomura Y, Wang Y. Color-tunable $LaCaAl_3O_7$:Ce^{3+},Tb^{3+} phosphors for UV light-emitting diodes. *Materials Research Bulletin*. 2013;48(1):114-117.

25. Qiao X, Fan X, Xue Z, Xu X. Short-wavelength upconversion luminescence of Yb^{3+}/Tm^{3+} co-doped glass ceramic containing SrF_2 nanocrystals. *Journal of Non-Crystalline Solids*. 2011;357(1):83-87.

26. Xu X, Yu X, Zhou D, Qiu J. A potential tunable blue-to-white-emitting phosphor CAO: Eu, Mn for ultraviolet light emitting diodes. *Materials Research Bulletin*. 2013;48:2390-2392.

27. Figueiredo MS, Santos FA, Yukimitu K, Moraes JCS, Nunes LAO, Andrade LHC, Lima SM. On observation of the downconversion mechanism in Er^{3+}/Yb^{3+} co-doped tellurite glass using thermal and optical parameters. *Journal of Luminescence*. 2015;157:365-370.